CMOS MEMS and their Simulation

Jan G. Korvink*, Markus Emmenegger, Stefano Taschini and Henry Baltes

* Institute for Microsystem Technology, University of Freiburg,
Am Flughafen 17, D-79110 Freiburg, Germany; korvink@informatik.uni-freiburg.de
Physical Electronics Laboratory, ETH Zurich,
CH-8093 Zurich, Switzerland; baltes@iqe.phys.ethz.ch

ABSTRACT

The most appropriate tools for the modelling and simulation of MEMS are strongly related to the technology used to fabricate them. CMOS MEMS are naturally combined with circuitry, and in a packaged form they are capable microsystems. The numerical models of the microsystems therefore have to include the domains and effects of the microsensors, microactuators, the CMOS circuitry and the packaging. To enable the use of such comprehensive models, we employ compact modelling techniques. The methods are removing the sharp distinction between "lumped" and "continuous" numerical models. This review illustrates recent work we have done in this area.

Keywords: CMOS, MEMS, Compact Model, Model Reduction, SPICE, Finite Element Method, Boundary Element Method.

INTRODUCTION

CMOS MEMS combine MEMS microdevices and CMOS circuitry into microsystems [1]. CMOS MEMS are fabricated using industrial CMOS foundry services. Industrial CMOS combined with process-compatible post-processing, such as anisotropic dry and wet etching of silicon, the removal of sacrificial dielectric or metal layers and selective deposition or plating and subsequent patterning of non-standard layers on the wafer surface, yields a wealth of possibilities for creating functioning MEMS.

This approach rewards the microsystem designer. CMOS fabrication facilities that provide ASIC services are less expensive than establishing a dedicated MEMS foundry. In addition, the full wealth of CMOS analogue and digital circuitry is available for interfacing with the microdevice.

The approach also has its challenges. CMOS foundry design rules must be adapted to the requirements of sensor and actuator devices. The signal-coupling material properties are typically not measured or monitored by the fab, and special techniques have to be developed to ensure reliable and functioning devices [2]. CMOS is optimized for electrical circuitry, thus CMOS MEMS designers have to cope with reduced possibilities when compared to dedicated MEMS processes.

Our design goal is always an optimized microsystem, thus comprehensive system-based modelling is required to save development resources. Many system level simulation languages and tools exist. Since CMOS MEMS are designed using mask layout tools, and the underlying electronic circuit design libraries are usually in SPICE netlist form, it is prudent to represent the microsystem also as a SPICE compact model netlist, and to extract the device netlist from the mask and process description.

The above facts partly motivate our current work. We therefore investigate methods to simulate entire microsystems. We prefer methods that consider as much detail as possible. Since detail is provided by tools such as the finite element method and boundary element method, we start here. The size of the simulation is usually the limiting factor.

In the first section we consider model reduction techniques [3]. For example, the physical dimensions of microsystems make the characteristic response times of thermal and mechanical phenomena comparable, requiring the coupled analysis of the system. We present a general method to investigate the frequency-domain behaviour of MEMS devices thermo-mechanically excited by an AC heating power. Characteristics of the method are the use of finite elements for the space-discretization and spectral analysis for the reduction of mechanical degrees of freedom.

We investigate methods to interface the more exact "continuous" numerical models to SPICE. In the second section we show how we generate consistent SPICE compact models of capacitive devices using discretization methods [4]. Currently we use the adaptive, accelerated multipole boundary element method to perform the spatial discretization. The capacitance matrix is extracted directly from the system matrix, without solving the associated linear system.

MODEL REDUCTION TECHNIQUES FOR THE FINITE ELEMENT METHOD

We consider a CMOS cantilever beam driven in resonance using a harmonically varying heating power. Used as a gas sensor, an adsorbing/absorbing thin film coating at the beam tip causes a weight-proportional shift in the resonance frequency of the beam [5]. The heat dissipated in a resistor causes a temperature rise at the base of the beam. Different thermal expansion coefficients in the beam sandwich lead to

a deflection of the beam.

Thermomechanical model

The behaviour of the beam sandwich is described using a thermo-viscoelastic constitutive model [6]. The conservation of momentum in a solid body is expressed by

$$\rho\ddot{u} = f + \nabla\cdot\sigma \tag{1}$$

where u is the unknown displacement vector field, ρ is specific mass of the body, and f is the resultant body force vector field. In a thermo-viscoelastic solid the stress tensor σ is related to the strain tensor ε through

$$\sigma = \lambda\mathrm{trace}(\varepsilon) + 2\mu\varepsilon + \eta\mathrm{trace}(\dot{\varepsilon}) + 2\zeta\dot{\varepsilon} \\ -(3\lambda + 2\mu)\alpha(T - T_0) \tag{2}$$

T and T_0 are the temperature distribution and the stress-free temperature fields. The material parameters μ and λ are the Lamé elasticity parameters, and η and ζ are the corresponding viscosity parameters. α is the coefficient of thermal expansion. The first order strain tensor ε is:

$$\varepsilon = [\nabla u + (\nabla u)^T]/2 \tag{3}$$

The energy balance is expressed in terms of the temperature T and the energy flux q as

$$\rho c_\varepsilon\dot{T} = -\nabla\cdot q \tag{4}$$

where c_ε is the constant strain thermal capacity. The energy flux consists of the heat flux related to the temperature gradient and that generated by the deformation work:

$$q = -\kappa\nabla T + (3\lambda + 2\mu)\alpha T_0\dot{u} \tag{5}$$

Heat conduction gives rise to thermoelastic damping in the system. Viscous forces account for the structural damping (internal friction). The weak form of equations (1), (2) and (5) are now discretized using the FEM, leading to a set of ordinary differential equations with respect to time:

$$M\ddot{u} + R\dot{u} + Au - BT = F_M \tag{6}$$

$$C\dot{T} - D\dot{u} + KT = F_T \tag{7}$$

We use the symbols u and T to denote the nodal displacement and temperature in the discretized system.

Harmonic Analysis

Harmonic analysis is used for the numerical investigation of the dynamic behaviour of the discretized system described by (6)-(7). The thermal harmonic analysis presented in [7] is generalized for the fully coupled equations of linear thermomechanics. Inserting the sinusoidal excitement

$$F_M(t) = F_M e^{j\omega t},\ F_T(t) = F_T e^{j\omega t} \tag{8}$$

and the response

$$u(t) = ue^{j\omega t},\ T(t) = Te^{j\omega t} \tag{9}$$

into the system (6)-(7) results in the algebraic equation

$$\begin{bmatrix} A - \omega^2 M + j\omega R & -B \\ -j\omega D & j\omega C + K \end{bmatrix} \begin{bmatrix} u \\ T \end{bmatrix} = \begin{bmatrix} F_M \\ F_T \end{bmatrix} \tag{10}$$

The order of this linear nonsymmetric complex-valued system is $4N$, where N denotes the number of computational nodes. Equation (10) is solved for the amplitude and phase of the displacement and temperature for variable ω.

Reduction by Spectral Analysis

Considered separately, the discretized, free, undamped mechanical system is characterized by the following set of ordinary differential equations

$$M\ddot{u} + Au = 0 \tag{11}$$

Assuming harmonic time-dependence of u

$$u(t) = u_\omega e^{j\omega t} \tag{12}$$

and inserting (12) into (11), yields

$$-\omega_i^2 Mu_i + Au_i = 0 \tag{13}$$

The solutions u_i of this equation are the eigenvectors of the mechanical system, the shapes of the modes of free vibration at the eigenfrequencies ω_i. The beam excitation frequencies are of the order of the first few modes, so that the mechanical system is well approximated by the lowest modes. The solution vector for the mechanical displacements is written as a superposition of the first n mechanical modes:

$$u = \sum_{i=1}^{n} v_i u_i \tag{14}$$

Inserting (14) into the Fourier-transformed thermomechanical equation (10) yields

$$\sum_{i=1}^{n} v_i[(\omega_i^2 - \omega^2)M + jR]u_i + BT = F_M \tag{15}$$

As long as $n < 3N$ this equation system has more equations than unknowns v_i. It is now projected onto the subspace spanned by the selected eigenmodes, yielding

$$\tilde{M}v + \tilde{B}T = \tilde{F}_M = u_j^T F_M \tag{16}$$

where the reduced matrices $\tilde{M}$ and $\tilde{B}$ are

$$\tilde{M}_{ij} = u_i^T[(\omega_j^2 - \omega^2)M + jR]u_j \tag{17}$$

$$\tilde{B}_{ij} = u_i^T\mathrm{row}_j(B) \tag{18}$$

For the thermal equation (11), it suffices to insert (14)

$$(j\omega C + K)T - j\omega\sum_{i=1}^{n} v_i Du_i = F_T. \tag{19}$$

With the reduced matrix

$$\tilde{D}_{ij} = \mathrm{row}_i(D)^T u_j \tag{20}$$

and combining (16), (19) and (20), we get

$$\begin{bmatrix} \tilde{M} & \tilde{B} \\ \tilde{D} & (j\omega C + K) \end{bmatrix} \begin{bmatrix} v \\ T \end{bmatrix} = \begin{bmatrix} \tilde{F}_M \\ F_T \end{bmatrix} \tag{21}$$

The number of unknowns is drastically reduced from $4N$ to $(N + n)$. Equation (21) is solved several times in a frequency sweep for ω, so that this form of spectral analysis results in a large saving of computational resources.

Results

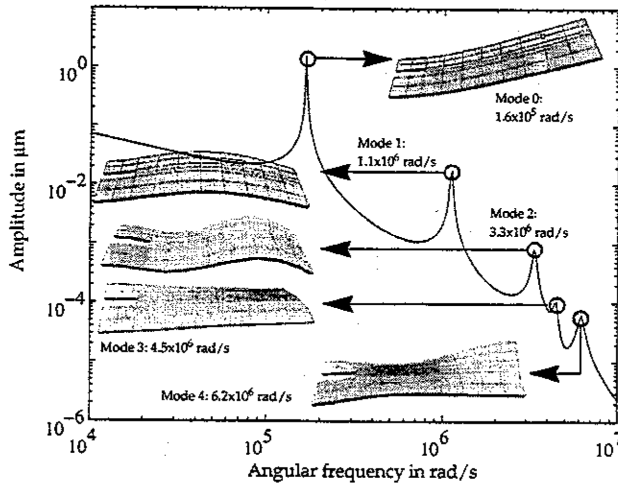

Figure 1. Computed beam tip amplitude as a function of excitation frequency for a heating power of $200mW$. The first five thermally-excited coupled mode shapes are shown.

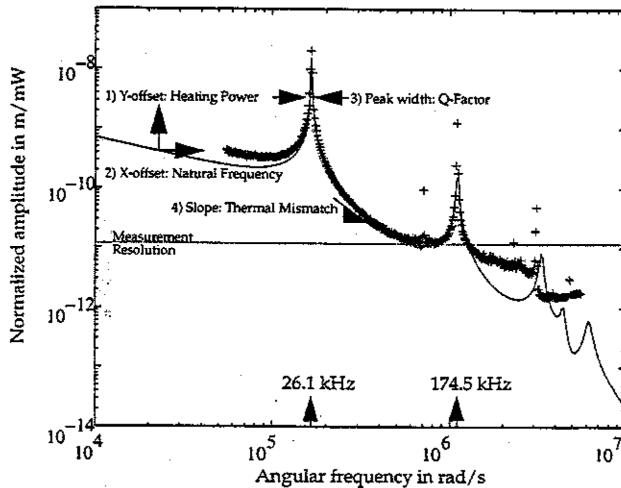

Figure 2. Computed (lines) and measured (+ symbols) normalized beam tip amplitude as a function of excitation frequency. The items 1) to 4) indicate the influence of an increase in parameter values on the shape of the response.

The computed fundamental frequency matches the measured values. The frequency response of the deflection at the tip of the beam is plotted in Figures 1 and 2, for the range of angular frequencies covered by the reduced mechanical spectrum for a heating power amplitude of 200 mW. We observe the following dependence of the mechanical response to device parameters (Figure 2): 1) The curve is shifted along the amplitude axis upon changing the heating power. 2) Changing the mechanical parameters shifts the entire curve along the frequency axis. 3) As expected, the width of the resonance peak depends on the beam's Q-factor, and therefore characterizes the damping ζ. 4) The mismatch of the thermal expansion coefficients in the bimorph beam changes the slope of the response curve between the resonant peaks. The figure of merit in designing the resonating beam is the ratio of amplitude to heating power u_t/P [8]. Given the geometry, the material parameters, and the Q factor, we now correctly compute the amplitude/heating power ratio.

COMPACT MODELS USING THE BOUNDARY ELEMENT METHOD

Current commercial tools for capacitance matrix extraction are based on the finite difference method (FDM) [9], the finite element method (FEM) [10], the finite volume method (FVM) [11], and the boundary element method (BEM) [12], [13], [14], [15], [16]. We limit the discussion to capacitance matrix extraction, however all results are equally applicable to resistance matrix extraction. In essence, each of the above tools employ the following algorithm for the extraction of the capacitance matrix:

Mesh the 3D geometry. The mesh introduces nodes, positions where the primitive variables are approximated. For electrostatics, the primitive variables are often chosen to be the nodal electrostatic potentials and the nodal fluxes (or surface charge densities).

Build a discrete linear system. The partial differential equation is projected onto a solution subspace using the weighted residual method. This results in a linear equation system, $Ay=b$, in terms of the unknown primitive variables y at the discrete node positions.

Solve $Ay=b$ once for each row of the capacitance matrix. For a geometry with m separate metallic conductors, solve m times. For solution j $(j=1,..m)$, the conductors i $(i = 1,..,m)$ are biased as $\psi_{ij}=\delta_{ij}$ Volt. The capacitance matrix values are extracted by integrating the computed surface charge densities over the surface of each conductor.

It is not necessary to solve the linear system $Ay=b$. The information on the capacitance matrix already resides in the linear system acquired using any of the above discretization methods. The linear system appears to be most efficiently obtained using the adaptive multipole accelerated BEM. This version of the BEM is hence used in the following work.

Other Work

It is possible to form a reduced-order compact model for the impedance (including inductance) directly from a 3D magnetoquasistatic discretization using a Krylov-subspace based method [17]. This approximation is accurate within a given excitation frequency range. Such a step is necessary when the initial physical model includes both resistive and reactive effects, leading to a complex-valued impedance. Alternatively, tensor analysis of networks applied to the partial element equivalent circuit (PEEC) [18] method can also be

used to achieve model reduction [19].

Direct Method using the BEM

The direct method of capacitance extraction proceeds according to the following algorithm:

Mesh the geometry. Using the process emulation methods, we compute geometry of the device and remesh for a minimal geometrical dielectric interface representation [20].

Build the linear system. With the adaptive multipole accelerated boundary element method we compute the coefficients of the linear system relating nodal voltages to nodal surface normal flux densities [21].

Eliminate internal variables. We eliminate the non-conductor variables from the linear system. The variables arise at inter-dielectric boundaries, homogeneous Neumann boundaries and from the intermediate variables of the multipole expansion.

Compact the system. We compact the linear system into a capacitance matrix using linear algebra techniques.

The BEM, including adaptivity [21] and multipole acceleration [14], results in the following discretized linear system for the electrostatic problem

$$H\psi = Gq \tag{22}$$

where G and H are square numerical coefficient matrices, ψ is a vector of nodal electrostatic potentials and q is a vector of nodal surface flux densities. We reorder and partition ψ and q, grouping the nodal variables that belong to each of the m conductors together

$$H\left[\psi_1 \ldots \psi_m\right]^T = G\left[q_1 \ldots q_m\right]^T \tag{23}$$

We introduce two new m-dimensional vectors, the conductor voltage vector V and the conductor charge vector Q. The relationships between V and ψ, and between Q and q, are as follows:

$$DV = \left[\psi_1 \ldots \psi_m\right]^T \tag{24}$$

$$Q = N\left[q_1 \ldots q_m\right]^T \tag{25}$$

The block diagonal rectangular matrix D is boolean and of dimension $(m \times n)$, marking the association of a mesh node with a conductor. The rectangular matrix N is a weighting matrix of dimension $(n \times m)$. Its entries are the area weights a_i for each node i, $(i=1,...,n)$, so that the product Nq forms the area integral of the charge density over the conductor surfaces. We define the inverse relationship of (25) using the pseudoinverse of N [22]:

$$\left[q_1 \ldots q_m\right]^T = (N^T(NN^T)^{-1})Q = N^+Q \tag{26}$$

We insert (26) into (23) to get

$$HDV = GN^+Q \tag{27}$$

The matrix product GN^+ is rectangular, and we also require its pseudoinverse:

$$(GN^+)^+ = ((GN^+)^T GN^+)^{-1}(GN^+)^T \tag{28}$$

Inserting (28) into (27) we get

$$(GN^+)^+ HDV = Q \tag{29}$$

or equivalently

$$CV = Q \tag{30}$$

where $C = (GN^+)^+ HD$ is the capacitance matrix for the m-conductor system relating conductor voltage to conductor charge.

Arbitrary boundary conditions and dielectrics

In the BEM for electrostatics, each mesh node corresponds to only one boundary region. The regions and their nodes have the following characteristics:

Dirichlet Boundary Regions. All the member nodes have the same prescribed conductor potential.

Neumann Boundary Regions. All the member nodes have the same prescribed surface-normal flux density (or surface charge density).

Floating Boundary Regions. All the member nodes have the same conductor potential, with a prescribed total charge on the conductor.

Interface Boundary Regions. The member nodes lie on interdielectric interfaces with known flux-potential relation.

Dirichlet and Floating boundaries are dealt with by the method of the previous section, by choosing an appropriate D and N matrix.

Homogeneous Neumann boundary conditions are useful devices to reduce the size of simulation geometries with inherent symmetries. These variables are eliminated from the equation system as detailed for internal interface boundary regions described below. Inhomogeneous Neumann boundary regions are not considered in our formulation.

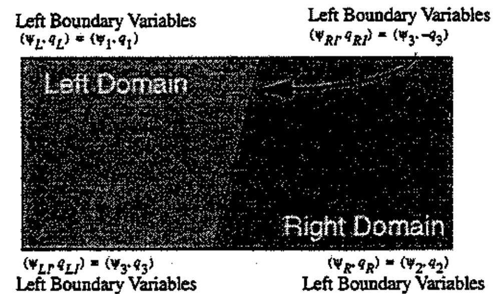

Figure 3. Partitioning into left, right and interface boundary regions.

To eliminate the variables lying on an interdielectric boundary region we first partition the simulation domain, and hence the equation system, to separate the interface, left and right variables (Figure 3). Here we treat a simple geometry, but the discussion is equally valid for geometries with multiple interfaces and domains, since interfaces are eliminated se-

quentially from the equation system.

For the Left domain boundary integral, relating the Left and Interface boundary variables, we get:

$$\begin{bmatrix} H_{11} & H_{13} \\ H_{31} & H_{33} \end{bmatrix} \begin{bmatrix} \psi_1 \\ \psi_3 \end{bmatrix} = \begin{bmatrix} G_{11} & G_{13} \\ G_{31} & G_{33} \end{bmatrix} \begin{bmatrix} q_1 \\ q_3 \end{bmatrix} \quad (31)$$

For the Right domain boundary integral, relating the Right and Interface boundary variables, we get:

$$\begin{bmatrix} H_{22} & H_{23} \\ H_{32} & H_{33} \end{bmatrix} \begin{bmatrix} \psi_2 \\ \psi_3 \end{bmatrix} = \begin{bmatrix} G_{22} & G_{23} \\ G_{32} & G_{33} \end{bmatrix} \begin{bmatrix} q_2 \\ q_3 \end{bmatrix} \quad (32)$$

Joining the systems for the Left and Right domains we get:

$$\begin{bmatrix} H_{11} & 0 & H_{13} \\ 0 & H_{22} & H_{23} \\ H_{31} & 0 & H_{33} \\ 0 & H_{32} & H_{33} \end{bmatrix} \begin{bmatrix} \psi_1 \\ \psi_2 \\ \psi_3 \end{bmatrix} = \begin{bmatrix} G_{11} & 0 & G_{13} \\ 0 & G_{22} & G_{23} \\ G_{31} & 0 & G_{33} \\ 0 & G_{32} & G_{33} \end{bmatrix} \begin{bmatrix} q_1 \\ q_2 \\ q_3 \end{bmatrix} \quad (33)$$

Simplifying, the reduced system becomes

$$\begin{bmatrix} \Gamma_{11} & \Gamma_{12} \\ H_{31} & -H_{32} \end{bmatrix} \begin{bmatrix} \psi_1 \\ \psi_2 \end{bmatrix} = \begin{bmatrix} \Xi_{11} & \Xi_{12} \\ G_{31} & -G_{32} \end{bmatrix} \begin{bmatrix} q_1 \\ q_2 \end{bmatrix} \quad (34)$$

with

$$\Gamma_{11} = (G_{23} - H_{23}H_{33}^{-1}G_{33})(H_{11} - H_{13}H_{33}^{-1}H_{31})$$
$$\Gamma_{12} = -(H_{22} - H_{23}H_{33}^{-1}H_{32})(G_{13} - H_{13}H_{33}^{-1}G_{33})$$
$$\Xi_{11} = (G_{23} - H_{23}H_{33}^{-1}G_{33})(G_{11} - H_{13}H_{33}^{-1}G_{31})$$
$$\Xi_{12} = -(G_{22} - H_{23}H_{33}^{-1}G_{32})(G_{13} - H_{13}H_{33}^{-1}G_{33})$$

Note that the effort to produce the reduced system is directly related to the size of discretization of the interfaces. The efficiency of the method depends on keeping the discretization of the interfaces to a minimal size.

Eliminating multipole expansion variables

The multipole expansion [14], employed in our algorithm introduces additional intermediate variables into the boundary element formalism which must be eliminated from the system. Let x denote the flux and potential variables, a the auxiliary variables introduced by the multipole expansion; the system reads

$$A_{11}x + A_{12}a = 0$$
$$A_{21}x + A_{22}a = 0 \quad (35)$$

The hierarchy of the multipole expansion algorithm results in a lower triangular A_{22} matrix, so that the auxiliary variables are easily eliminated from the system. Taking the Schur complement of the block A_{22}, system (35) is transformed into

$$(A_{11} - A_{12}A_{22}^{-1}A_{21})x = 0, \quad (36)$$

where the cost of the computation of $A_{22}^{-1}A_{21}$ is that of one back-substitution times the number of columns of A_{21}.

Results

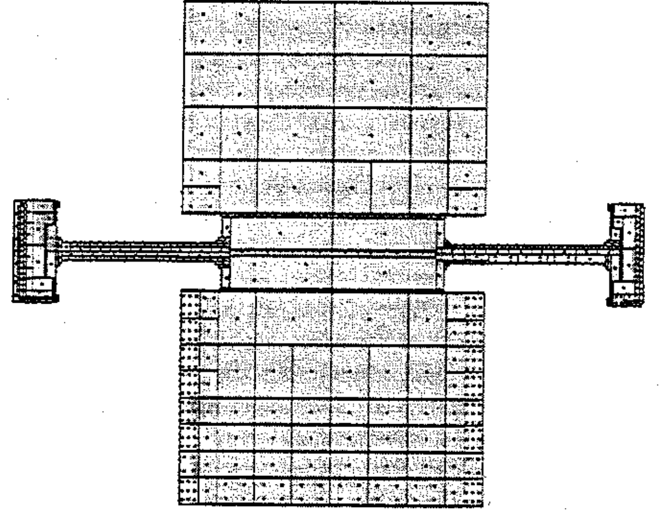

Figure 4. Surface mesh of the CMOS MEMS micromirror suitable for simulation with the boundary element method. The red dots indicate the nodes (collocation points) of each element of the mesh. The mesh represents 2120 quadrilateral panel elements, 2414 collocation nodes, 5088 multipole variables and ca. 5×10^6 non-zero matrix entries [16], [20].

We consider a MEMS micromirror, fabricated using an industrial CMOS process combined with post-CMOS micromachining [23]. The aluminum mirror, suspended by two beam hinges, is actuated to rotate about the hinges using electrodes placed underneath the mirror surface. Two additional landing electrodes prevent the electrostatic adhesion of the mirror to the substrate. The generation of the computational geometry illustrated in Figure 4 is dealt with in [21]. We computed the capacitance matrix for the mirror for a range of mirror deflection angles from 0° to 4.1° and plotted in Figure 5. Computing the 5×5 capacitance matrix using the compaction method presented here requires an average of 824 seconds on a SPARC Ultra 2 workstation.

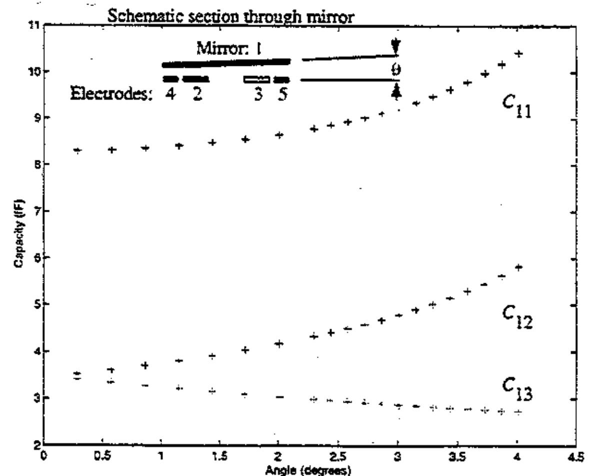

Figure 5. Plot of the first row terms of the capacitance matrix vs. angle for the CMOS MEMS micromirror.

CONCLUSIONS

Numerical techniques such as the finite element method and the boundary element method are powerful tools with which to investigate the nonlinear, time-dependent behaviour of coupled physics in MEMS devices. Microsystems consist of these devices, together with circuit elements and packaging solutions. The whole ensemble can have complex cross-talk mechanisms which must be understood when designing reliable microsystems. We investigate methods to bridge the gap between the "continuous" numerical methods and the compact "discrete" network simulators. We have performed the coupled harmonic analysis of a thermomechanically actuated gas sensor under development in our laboratory. Our method uses finite elements for the space-discretization, and spectral analysis for system reduction. We routinely investigate the frequency-domain behaviour of MEMS devices excited by an AC heating power, and correctly determine the amplitude/heating power ratio, given the damping factor, the geometry, and the material parameters. The capacitance extraction method detailed here exploits the accuracy of the boundary element method to compute the compact model influence matrix of a multiconductor interconnect directly, without resorting to explicitly solving the linear system. The method works for arbitrary geometrical configurations in 2 and 3 space dimensions, with an arbitrary number of dielectric materials, prescribed voltage conductors, prescribed charge conductors and symmetry planes.

ACKNOWLEDGEMENTS

We thank Dirk Lange, Mark Hornung and Dr. Oliver Paul for the experimental data and discussions, Dr. Andreas Greiner for discussions and Dr. Martin Bächtold of Coyote Systems for numerous invigorating discussions regarding the adaptive, multipole accelerated boundary element method. We also thank Dr. Lars Bomholt, Dr. Hans-Petter Lien of ISE Integrated Systems Engineering AG, Zurich and Mr. Götz Leonhardt of the Integrated Systems Laboratory, ETH Zurich for many discussions surrounding the benchmarking of capacitance extraction methods, as well as the input geometries for the interconnect example. Special thanks also goes to Dr. Roland Rühl and Dr. Diederik Fokkema of ISE Integrated Systems Engineering AG, Zurich.

The first part of this work is supported by the Swiss Priority Program MINAST.

REFERENCES

1. A. Häberli, H. Baltes (Invited Review), "CMOS MEMS", Proc. IEEE Int. Symp. Circ. Syst. (ISCAS), Hong Kong (1997) 2813-2816
2. H. Baltes, O. Paul, J. G. Korvink, "Simulation Toolbox and Material Parameter Data Base for CMOS MEMS", Proc. 7th Intl. Symposium on Micro Machine and Human Science (MHS '96), Tokyo (1996) 1-8
3. M. Emmenegger, S. Taschini, J. G. Korvink, and H. Baltes, Simulation of a Thermomechanically Actuated Gas Sensor, Proc. IEEE Int. Workshop on Micro Electro Mechanical Systems (MEMS), Heidelberg (1998) 184-189
4. J. G. Korvink, S. Taschini, H. Baltes, An Efficient Direct Method for the Determination of 3D Interconnect Compact Model Capacitances, Submitted to IEEE Trans. on CAD of Integrated Circuits and Systems (1998)
5. H. Baltes, A. Koll, D. Lange, "The CMOS MEMS Nose - Fact or Fiction?", Proceedings of the IEEE International Symposium on Industrial Electronics ISIE '97 (1997) SS152 - SS157
6. L.D. Landau, E.M. Lifshitz, "Theory of Elasticity", Pergamon Press, Oxford
7. M. Emmenegger, J. G. Korvink, M. Bächtold, O. Paul, M. von Arx, J. Funk, H. Baltes, "Application of Harmonic Finite Element Analysis to a CMOS Heat-capacity Measurement Structure", *CAD for MEMS 96, Zurich* (1996)
8. O. Brand, "Micromachined Resonators for Ultrasound Based Proximity Sensing", Ph.D. Thesis, ETH Zurich No. 10896, Zurich, Switzerland (1994)
9. Technology Modeling Associates Inc., RAPHAEL, Sunnyvale, CA
10. ISE Integrated Systems Engineering AG, "Modeling of Semiconductor Technology, Devices and Systems", SOLIDIS Reference Manual, Zurich (1995)
11. ISE Integrated Systems Engineering AG, "Modeling of Semiconductor Technology, Devices and Systems", DESSIS Reference Manual, Zurich (1995)
12. A. E. Ruehli and P. A. Brennan, "Efficient Capacitance Calculations for Three-Dimensional Multiconductor Systems", IEEE Transactions on Microwave Theory and Techniques, 21 (1973) 76-82
13. K. Nabors, F.T. Korsmeyer, F.T. Leighton and J. White, "Preconditioned, Adaptive, Multipole-Accelerated Iterative Methods for 3D First-Kind Integral Equations of Potential Theory", SIAM J. Sci. Stat. Comput., 15 (1994)
14. M. Bächtold, J.G. Korvink and H. Baltes, "Enhanced Multipole Acceleration Technique for the Solution of Large Poisson Computations", IEEE Trans. on CAD of Integrated Circuits and Systems, 15 (1996) 1541-1546
15. M. Bächtold, M. Emmenegger, J.G. Korvink and H. Baltes, "An Error Indicator and Automatic Adaptive Meshing for Electrostatic Boundary Element Simulations", IEEE Trans. on CAD of Integrated Circuits and Systems (1997)
16. M. Bächtold, S. Taschini, J. G. Korvink, and H. Baltes, "Automated Extraction of Capacitances and Electrostatic Forces in MEMS and ULSI Interconnects from the Mask Layout", Proc. IEDM, Washington (1997)129-132
17. L.M. Silveira, M. Kamon, J. White, "Efficient Reduced-Order Modeling of Frequency-Dependent Coupling Inductances Associated with 3-D Interconnect Structures", IEEE Trans. on Components, Hybrids, and Manufacturing Technology, Part B: Advanced Packaging, 19 (1996) 283-288
18. A. Ruehli, "Circuit Oriented EM Modeling Techniques for EMC", Proceedings EMC'97, Zurich (1997) 509-514
19. G. Coen, D. De Zutter, "Reduction of Circuit Complexity Using Tensor Analysis of Networks", Proceedings EMC'97, Zurich (1997) 535-540
20. M. Bächtold, J. G. Korvink and H. Baltes, "Automatic Adaptive Meshing for Efficient Electrostatic Boundary Element Simulations", Proc. SISPAD, IEEE (1996) 127-128
21. M. Bächtold, "Efficient 3D Computation of Electrostatic Fields and Forces in Microsystems", Ph.D. Thesis, ETH Zurich, Physical Electronics Laboratory (1997)
22. R. Penrose, "A generalized inverse for matrices", Proc. Cambridge Phil. Soc., 51 (1955) 406-413
23. J. Bühler, J. Funk, J.G. Korvink, H. Baltes, "Electrostatic Aluminum Micromirrors using Double Pass Metallization", IEEE J. of Micro-Electro-Mechanical Systems (1997)126-135